Search for intermediate resonances and dark gauge bosons in $J/\psi \to \gamma\pi^0\eta'$

M. Ablikim,[1] M. N. Achasov,[10,d] P. Adlarson,[59] S. Ahmed,[15] M. Albrecht,[4] M. Alekseev,[58a,58c] A. Amoroso,[58a,58c] F. F. An,[1] Q. An,[55,43] Y. Bai,[42] O. Bakina,[27] R. Baldini Ferroli,[23a] I. Balossino,[24a] Y. Ban,[35,l] K. Begzsuren,[25] J. V. Bennett,[5] N. Berger,[26] M. Bertani,[23a] D. Bettoni,[24a] F. Bianchi,[58a,58c] J. Biernat,[59] J. Bloms,[52] I. Boyko,[27] R. A. Briere,[5] H. Cai,[60] X. Cai,[1,43] A. Calcaterra,[23a] G. F. Cao,[1,47] N. Cao,[1,47] S. A. Cetin,[46b] J. Chai,[58c] J. F. Chang,[1,43] W. L. Chang,[1,47] G. Chelkov,[27,b,c] D. Y. Chen,[6] G. Chen,[1] H. S. Chen,[1,47] J. Chen,[16] J. C. Chen,[1] M. L. Chen,[1,43] S. J. Chen,[33] Y. B. Chen,[1,43] W. Cheng,[58c] G. Cibinetto,[24a] F. Cossio,[58c] X. F. Cui,[34] H. L. Dai,[1,43] J. P. Dai,[38,h] X. C. Dai,[1,47] A. Dbeyssi,[15] D. Dedovich,[27] Z. Y. Deng,[1] A. Denig,[26] I. Denysenko,[27] M. Destefanis,[58a,58c] F. De Mori,[58a,58c] Y. Ding,[31] C. Dong,[34] J. Dong,[1,43] L. Y. Dong,[1,47] M. Y. Dong,[1,43,47] Z. L. Dou,[33] S. X. Du,[63] J. Z. Fan,[45] J. Fang,[1,43] S. S. Fang,[1,47] Y. Fang,[1] R. Farinelli,[24a,24b] L. Fava,[58b,58c] F. Feldbauer,[4] G. Felici,[23a] C. Q. Feng,[55,43] M. Fritsch,[4] C. D. Fu,[1] Y. Fu,[1] Q. Gao,[1] X. L. Gao,[55,43] Y. Gao,[45] Y. Gao,[56] Y. G. Gao,[6] Z. Gao,[55,43] B. Garillon,[26] I. Garzia,[24a] E. M. Gersabeck,[50] A. Gilman,[51] K. Goetzen,[11] L. Gong,[34] W. X. Gong,[1,43] W. Gradl,[26] M. Greco,[58a,58c] L. M. Gu,[33] M. H. Gu,[1,43] S. Gu,[2] Y. T. Gu,[13] A. Q. Guo,[22] L. B. Guo,[32] R. P. Guo,[36] Y. P. Guo,[26] A. Guskov,[27] S. Han,[60] X. Q. Hao,[16] F. A. Harris,[48] K. L. He,[1,47] F. H. Heinsius,[4] T. Held,[4] Y. K. Heng,[1,43,47] M. Himmelreich,[11,g] Y. R. Hou,[47] Z. L. Hou,[1] H. M. Hu,[1,47] J. F. Hu,[38,h] T. Hu,[1,43,47] Y. Hu,[1] G. S. Huang,[55,43] J. S. Huang,[16] X. T. Huang,[37] X. Z. Huang,[33] N. Huesken,[52] T. Hussain,[57] W. Ikegami Andersson,[59] W. Imoehl,[22] M. Irshad,[55,43] Q. Ji,[1] Q. P. Ji,[16] X. B. Ji,[1,47] X. L. Ji,[1,43] H. L. Jiang,[37] X. S. Jiang,[1,43,47] X. Y. Jiang,[34] J. B. Jiao,[37] Z. Jiao,[18] D. P. Jin,[1,43,47] S. Jin,[33] Y. Jin,[49] T. Johansson,[59] N. Kalantar-Nayestanaki,[29] X. S. Kang,[31] R. Kappert,[29] M. Kavatsyuk,[29] B. C. Ke,[1] I. K. Keshk,[4] A. Khoukaz,[52] P. Kiese,[26] R. Kiuchi,[1] R. Kliemt,[11] L. Koch,[28] O. B. Kolcu,[46b,f] B. Kopf,[4] M. Kuemmel,[4] M. Kuessner,[4] A. Kupsc,[59] M. Kurth,[1] M. G. Kurth,[1,47] W. Kühn,[28] J. S. Lange,[28] P. Larin,[15] L. Lavezzi,[58c] H. Leithoff,[26] T. Lenz,[26] C. Li,[59] Cheng Li,[55,43] D. M. Li,[63] F. Li,[1,43] F. Y. Li,[35,l] G. Li,[1] H. B. Li,[1,47] H. J. Li,[9,j] J. C. Li,[1] J. W. Li,[41] Ke Li,[1] L. K. Li,[1] Lei Li,[3] P. L. Li,[55,43] P. R. Li,[30] Q. Y. Li,[37] W. D. Li,[1,47] W. G. Li,[1] X. H. Li,[55,43] X. L. Li,[37] X. N. Li,[1,43] Z. B. Li,[44] Z. Y. Li,[44] H. Liang,[1,47] H. Liang,[55,43] Y. F. Liang,[40] Y. T. Liang,[28] G. R. Liao,[12] L. Z. Liao,[1,47] J. Libby,[21] C. X. Lin,[44] D. X. Lin,[15] Y. J. Lin,[13] B. Liu,[38,h] B. J. Liu,[1] C. X. Liu,[1] D. Liu,[55,43] D. Y. Liu,[38,h] F. H. Liu,[39] Fang Liu,[1] Feng Liu,[6] H. B. Liu,[13] H. M. Liu,[1,47] Huanhuan Liu,[1] Huihui Liu,[17] J. B. Liu,[55,43] J. Y. Liu,[1,47] K. Y. Liu,[31] Ke Liu,[6] L. Y. Liu,[13] Q. Liu,[47] S. B. Liu,[55,43] T. Liu,[1,47] X. Liu,[30] X. Y. Liu,[1,47] Y. B. Liu,[34] Z. A. Liu,[1,43,47] Zhiqing Liu,[37] Y. F. Long,[35,l] X. C. Lou,[1,43,47] H. J. Lu,[18] J. D. Lu,[1,47] J. G. Lu,[1,43] Y. Lu,[1] Y. P. Lu,[1,43] C. L. Luo,[32] M. X. Luo,[62] P. W. Luo,[44] T. Luo,[9,j] X. L. Luo,[1,43] S. Lusso,[58c] X. R. Lyu,[47] F. C. Ma,[31] H. L. Ma,[1] L. L. Ma,[37] M. M. Ma,[1,47] Q. M. Ma,[1] X. N. Ma,[34] X. X. Ma,[1,47] X. Y. Ma,[1,43] Y. M. Ma,[37] F. E. Maas,[15] M. Maggiora,[58a,58c] S. Maldaner,[26] S. Malde,[53] Q. A. Malik,[57] A. Mangoni,[23b] Y. J. Mao,[35,l] Z. P. Mao,[1] S. Marcello,[58a,58c] Z. X. Meng,[49] J. G. Messchendorp,[29] G. Mezzadri,[24a] J. Min,[1,43] T. J. Min,[33] R. E. Mitchell,[22] X. H. Mo,[1,43,47] Y. J. Mo,[6] C. Morales Morales,[15] N. Yu. Muchnoi,[10,d] H. Muramatsu,[51] A. Mustafa,[4] S. Nakhoul,[11,g] Y. Nefedov,[27] F. Nerling,[11,g] I. B. Nikolaev,[10,d] Z. Ning,[1,43] S. Nisar,[8,k] S. L. Niu,[1,43] S. L. Olsen,[47] Q. Ouyang,[1,43,47] S. Pacetti,[23b] Y. Pan,[55,43] M. Papenbrock,[59] P. Patteri,[23a] M. Pelizaeus,[4] H. P. Peng,[55,43] K. Peters,[11,g] J. Pettersson,[59] J. L. Ping,[32] R. G. Ping,[1,47] A. Pitka,[4] R. Poling,[51] V. Prasad,[55,43] H. R. Qi,[2] M. Qi,[33] T. Y. Qi,[2] S. Qian,[1,43] C. F. Qiao,[47] N. Qin,[60] X. P. Qin,[13] X. S. Qin,[4] Z. H. Qin,[1,43] J. F. Qiu,[1] S. Q. Qu,[34] K. H. Rashid,[57,i] K. Ravindran,[21] C. F. Redmer,[26] M. Richter,[4] A. Rivetti,[58c] V. Rodin,[29] M. Rolo,[58c] G. Rong,[1,47] Ch. Rosner,[15] M. Rump,[52] A. Sarantsev,[27,e] M. Savrié,[24b] Y. Schelhaas,[26] K. Schoenning,[59] W. Shan,[19] X. Y. Shan,[55,43] M. Shao,[55,43] C. P. Shen,[2] P. X. Shen,[34] X. Y. Shen,[1,47] H. Y. Sheng,[1] X. Shi,[1,43] X. D. Shi,[55,43] J. J. Song,[37] Q. Q. Song,[55,43] X. Y. Song,[1] S. Sosio,[58a,58c] C. Sowa,[4] S. Spataro,[58a,58c] F. F. Sui,[37] G. X. Sun,[1] J. F. Sun,[16] L. Sun,[60] S. S. Sun,[1,47] X. H. Sun,[1] Y. J. Sun,[55,43] Y. K. Sun,[55,43] Y. Z. Sun,[1] Z. J. Sun,[1,43] Z. T. Sun,[1] Y. T. Tan,[55,43] C. J. Tang,[40] G. Y. Tang,[1] X. Tang,[1] V. Thoren,[59] B. Tsednee,[25] I. Uman,[46d] B. Wang,[1] B. L. Wang,[47] C. W. Wang,[33] D. Y. Wang,[35,l] K. Wang,[1,43] L. L. Wang,[1] L. S. Wang,[1] M. Wang,[37] M. Z. Wang,[35,l] Meng Wang,[1,47] P. L. Wang,[1] R. M. Wang,[61] W. P. Wang,[55,43] X. Wang,[35,l] X. F. Wang,[1] X. L. Wang,[9,j] Y. Wang,[55,43] Y. Wang,[44] Y. F. Wang,[1,43,47] Y. Q. Wang,[1] Z. Wang,[1,43] Z. G. Wang,[1,43] Z. Y. Wang,[1] Zongyuan Wang,[1,47] T. Weber,[4] D. H. Wei,[12] P. Weidenkaff,[26] H. W. Wen,[32] S. P. Wen,[1] U. Wiedner,[4] G. Wilkinson,[53] M. Wolke,[59] L. H. Wu,[1] L. J. Wu,[1,47] Z. Wu,[1,43] L. Xia,[55,43] Y. Xia,[20] S. Y. Xiao,[1] Y. J. Xiao,[1,47] Z. J. Xiao,[32] Y. G. Xie,[1,43] Y. H. Xie,[6] T. Y. Xing,[1,47] X. A. Xiong,[1,47] Q. L. Xiu,[1,43] G. F. Xu,[1] J. J. Xu,[33] L. Xu,[1] Q. J. Xu,[14] W. Xu,[1,47] X. P. Xu,[41] F. Yan,[56] L. Yan,[58a,58c] W. B. Yan,[55,43] W. C. Yan,[2] Y. H. Yan,[20] H. J. Yang,[38,h] H. X. Yang,[1] L. Yang,[60] R. X. Yang,[55,43] S. L. Yang,[1,47] Y. H. Yang,[33] Y. X. Yang,[12] Yifan Yang,[1,47] Z. Q. Yang,[20] M. Ye,[1,43] M. H. Ye,[7] J. H. Yin,[1] Z. Y. You,[44] B. X. Yu,[1,43,47] C. X. Yu,[34] J. S. Yu,[20] T. Yu,[56] C. Z. Yuan,[1,47] X. Q. Yuan,[35,l] Y. Yuan,[1] A. Yuncu,[46b,a] A. A. Zafar,[57] Y. Zeng,[20] B. X. Zhang,[1] B. Y. Zhang,[1,43] C. C. Zhang,[1] D. H. Zhang,[1] H. H. Zhang,[44] H. Y. Zhang,[1,43] J. Zhang,[1,47] J. L. Zhang,[61] J. Q. Zhang,[4] J. W. Zhang,[1,43,47] J. Y. Zhang,[1] J. Z. Zhang,[1,47] K. Zhang,[1,47] L. Zhang,[33] L. Zhang,[45] S. F. Zhang,[33] T. J. Zhang,[38,h] X. Y. Zhang,[37] Y. Zhang,[55,43] Y. H. Zhang,[1,43] Y. T. Zhang,[55,43] Yang Zhang,[1] Yao Zhang,[1] Yi Zhang,[9,j] Yu Zhang,[47] Z. H. Zhang,[6] Z. P. Zhang,[55] Z. Y. Zhang,[60] G. Zhao,[1]

J. W. Zhao,[1,43] J. Y. Zhao,[1,47] J. Z. Zhao,[1,43] Lei Zhao,[55,43] Ling Zhao,[1] M. G. Zhao,[34] Q. Zhao,[1] S. J. Zhao,[63] T. C. Zhao,[1] Y. B. Zhao,[1,43] Z. G. Zhao,[55,43] A. Zhemchugov,[27,b] B. Zheng,[56] J. P. Zheng,[1,43] Y. Zheng,[35,l] Y. H. Zheng,[47] B. Zhong,[32] L. Zhou,[1,43] L. P. Zhou,[1,47] Q. Zhou,[1,47] X. Zhou,[60] X. K. Zhou,[47] X. R. Zhou,[55,43] Xiaoyu Zhou,[20] Xu Zhou,[20] A. N. Zhu,[1,47] J. Zhu,[34] J. Zhu,[44] K. Zhu,[1] K. J. Zhu,[1,43,47] S. H. Zhu,[54] W. J. Zhu,[34] X. L. Zhu,[45] Y. C. Zhu,[55,43] Y. S. Zhu,[1,47] Z. A. Zhu,[1,47] J. Zhuang,[1,43] B. S. Zou,[1] and J. H. Zou[1]

(BESIII Collaboration)

[1]*Institute of High Energy Physics, Beijing 100049, People's Republic of China*
[2]*Beihang University, Beijing 100191, People's Republic of China*
[3]*Beijing Institute of Petrochemical Technology, Beijing 102617, People's Republic of China*
[4]*Bochum Ruhr-University, D-44780 Bochum, Germany*
[5]*Carnegie Mellon University, Pittsburgh, Pennsylvania 15213, USA*
[6]*Central China Normal University, Wuhan 430079, People's Republic of China*
[7]*China Center of Advanced Science and Technology, Beijing 100190, People's Republic of China*
[8]*COMSATS University Islamabad, Lahore Campus, Defence Road, Off Raiwind Road, 54000 Lahore, Pakistan*
[9]*Fudan University, Shanghai 200443, People's Republic of China*
[10]*G.I. Budker Institute of Nuclear Physics SB RAS (BINP), Novosibirsk 630090, Russia*
[11]*GSI Helmholtzcentre for Heavy Ion Research GmbH, D-64291 Darmstadt, Germany*
[12]*Guangxi Normal University, Guilin 541004, People's Republic of China*
[13]*Guangxi University, Nanning 530004, People's Republic of China*
[14]*Hangzhou Normal University, Hangzhou 310036, People's Republic of China*
[15]*Helmholtz Institute Mainz, Johann-Joachim-Becher-Weg 45, D-55099 Mainz, Germany*
[16]*Henan Normal University, Xinxiang 453007, People's Republic of China*
[17]*Henan University of Science and Technology, Luoyang 471003, People's Republic of China*
[18]*Huangshan College, Huangshan 245000, People's Republic of China*
[19]*Hunan Normal University, Changsha 410081, People's Republic of China*
[20]*Hunan University, Changsha 410082, People's Republic of China*
[21]*Indian Institute of Technology Madras, Chennai 600036, India*
[22]*Indiana University, Bloomington, Indiana 47405, USA*
[23a]*INFN Laboratori Nazionali di Frascati, I-00044, Frascati, Italy*
[23b]*INFN and University of Perugia, I-06100, Perugia, Italy*
[24a]*INFN Sezione di Ferrara, I-44122, Ferrara, Italy*
[24b]*University of Ferrara, I-44122, Ferrara, Italy*
[25]*Institute of Physics and Technology, Peace Avenue 54B, Ulaanbaatar 13330, Mongolia*
[26]*Johannes Gutenberg University of Mainz, Johann-Joachim-Becher-Weg 45, D-55099 Mainz, Germany*
[27]*Joint Institute for Nuclear Research, 141980 Dubna, Moscow region, Russia*
[28]*Justus-Liebig-Universitaet Giessen, II. Physikalisches Institut, Heinrich-Buff-Ring 16, D-35392 Giessen, Germany*
[29]*KVI-CART, University of Groningen, NL-9747 AA Groningen, Netherlands*
[30]*Lanzhou University, Lanzhou 730000, People's Republic of China*
[31]*Liaoning University, Shenyang 110036, People's Republic of China*
[32]*Nanjing Normal University, Nanjing 210023, People's Republic of China*
[33]*Nanjing University, Nanjing 210093, People's Republic of China*
[34]*Nankai University, Tianjin 300071, People's Republic of China*
[35]*Peking University, Beijing 100871, People's Republic of China*
[36]*Shandong Normal University, Jinan 250014, People's Republic of China*
[37]*Shandong University, Jinan 250100, People's Republic of China*
[38]*Shanghai Jiao Tong University, Shanghai 200240, People's Republic of China*
[39]*Shanxi University, Taiyuan 030006, People's Republic of China*
[40]*Sichuan University, Chengdu 610064, People's Republic of China*
[41]*Soochow University, Suzhou 215006, People's Republic of China*
[42]*Southeast University, Nanjing 211100, People's Republic of China*
[43]*State Key Laboratory of Particle Detection and Electronics, Beijing 100049, Hefei 230026, People's Republic of China*
[44]*Sun Yat-Sen University, Guangzhou 510275, People's Republic of China*
[45]*Tsinghua University, Beijing 100084, People's Republic of China*
[46a]*Ankara University, 06100 Tandogan, Ankara, Turkey*

[46b]Istanbul Bilgi University, 34060 Eyup, Istanbul, Turkey
[46c]Uludag University, 16059 Bursa, Turkey
[46d]Near East University, Nicosia, North Cyprus, Mersin 10, Turkey
[47]University of Chinese Academy of Sciences, Beijing 100049, People's Republic of China
[48]University of Hawaii, Honolulu, Hawaii 96822, USA
[49]University of Jinan, Jinan 250022, People's Republic of China
[50]University of Manchester, Oxford Road, Manchester M13 9PL, United Kingdom
[51]University of Minnesota, Minneapolis, Minnesota 55455, USA
[52]University of Muenster, Wilhelm-Klemm-Strasse 9, 48149 Muenster, Germany
[53]University of Oxford, Keble Road, Oxford OX13RH, United Kingdom
[54]University of Science and Technology Liaoning, Anshan 114051, People's Republic of China
[55]University of Science and Technology of China, Hefei 230026, People's Republic of China
[56]University of South China, Hengyang 421001, People's Republic of China
[57]University of the Punjab, Lahore 54590, Pakistan
[58a]University of Turin, I-10125, Turin, Italy
[58b]University of Eastern Piedmont, I-15121, Alessandria, Italy
[58c]INFN, I-10125, Turin, Italy
[59]Uppsala University, Box 516, SE-75120 Uppsala, Sweden
[60]Wuhan University, Wuhan 430072, People's Republic of China
[61]Xinyang Normal University, Xinyang 464000, People's Republic of China
[62]Zhejiang University, Hangzhou 310027, People's Republic of China
[63]Zhengzhou University, Zhengzhou 450001, People's Republic of China

(Received 19 February 2020; accepted 25 August 2020; published 17 September 2020)

We report on an analysis of the decay $J/\psi \to \gamma\pi^0\eta'$ using a sample of $(1310.6 \pm 7.0) \times 10^6 J/\psi$ events collected with the BESIII detector. We search for the CP-violating process $\eta_c \to \pi^0\eta'$ and a dark gauge boson U' in $J/\psi \to U'\eta', U' \to \gamma\pi^0, \pi^0 \to \gamma\gamma$. No evidence of an η_c signal is observed in the $\pi^0\eta'$ invariant-mass spectrum and the upper limit of the branching fraction is determined to be 5.6×10^{-5} at the 90% confidence level. We also find no evidence of U' production and set upper limits at the 90% confidence level on the product branching fraction $\mathcal{B}(J/\psi \to U'\eta') \times \mathcal{B}(U' \to \pi^0\gamma)$ in the range between $(0.8 - 6.5) \times 10^{-7}$ for $0.2 \le m_{U'} \le 2.1$ GeV/c^2. In addition, we study the process $J/\psi \to \omega\eta'$ with $\omega \to \gamma\pi^0$. The branching fraction of $J/\psi \to \omega\eta'$ is found to be $(1.87 \pm 0.09 \pm 0.12) \times 10^{-4}$, where the first uncertainty is statistical and the second is systematic, with a precision that is improved by a factor of 1.4 over the previously published BESIII measurement.

DOI: 10.1103/PhysRevD.102.052005

[a]Also at Bogazici University, 34342 Istanbul, Turkey.
[b]Also at Moscow Institute of Physics and Technology, Moscow 141700, Russia.
[c]Also at Functional Electronics Laboratory, Tomsk State University, Tomsk, 634050, Russia.
[d]Also at Novosibirsk State University, Novosibirsk, 630090, Russia.
[e]Also at NRC "Kurchatov Institute," PNPI, 188300, Gatchina, Russia.
[f]Also at Istanbul Arel University, 34295 Istanbul, Turkey.
[g]Also at Goethe University Frankfurt, 60323 Frankfurt am Main, Germany.
[h]Also at Key Laboratory for Particle Physics, Astrophysics and Cosmology, Ministry of Education; Shanghai Key Laboratory for Particle Physics and Cosmology; Institute of Nuclear and Particle Physics, Shanghai 200240, People's Republic of China.
[i]Also at Government College Women University, Sialkot—51310, Punjab, Pakistan.
[j]Also at Key Laboratory of Nuclear Physics and Ion-beam Application (MOE) and Institute of Modern Physics, Fudan University, Shanghai 200443, People's Republic of China.
[k]Also at Department of Physics, Harvard University, Cambridge, MA, 02138, USA.
[l]Also at State Key Laboratory of Nuclear Physics and Technology, Peking University, Beijing 100871, People's Republic of China.

I. INTRODUCTION

The Standard Model (SM) has been successful in explaining a wide variety of experimental data; however it fails to explain several observations, such as dark matter, the baryon asymmetry in the Universe, the neutrino masses, and so on. Therefore, in recent years the search for new physics beyond the SM is one of the important activities of particle physicists worldwide. The BESIII (Beijing Electron Spectrometer) experiment is currently searching for beyond-the-SM physics using low-energy e^+e^- collision data. This is complementary to experiments conducted at the Large Hadron Collider (LHC) at CERN, which use high-energy hadron collision data. Huge data samples accumulated by the BESIII detector and taken at center-of-mass energies corresponding to the masses of various charmonium resonances [J/ψ, $\psi(3686)$ and $\psi(3770)$] offer a unique sensitivity to search for forbidden decays and dark matter particles in the low-energy region [1].

Charge conjugation and parity symmetry (CP) violation has only been observed in weak interactions, which in the SM, originates from a single complex phase in the Cabibbo-Kobayashi-Maskawa (CKM) quark-mixing matrix [2]. Therefore, searches for this phenomenon will provide new insights and will help to determine whether the phase in the CKM mixing matrix is the sole source of CP violation or whether there are other sources. The production of heavy pseudoscalar mesons, e.g., η, η', and η_c, in J/ψ decays offers an opportunity to test this fundamental symmetry. In the SM, the decays of $\eta/\eta' \to \pi\pi$ can proceed only via the weak interactions and the expected branching fractions are at a level of 10^{-29}–10^{-27} [3], which are experimentally inaccessible. In the case of the CP violation taking place in an extended Higgs sector [3], the branching fraction of $\eta \to \pi\pi$ may reach the level of 10^{-12}, which is considerably larger than the expectation in the SM. The decay of an η_c ($J^{PC} = 0^{-+}$) to two pseudoscalar mesons is forbidden due to CP conservation. The observation of these forbidden decays will be a clear indication of new physics beyond the SM. Using a sample of 225 million J/ψ events, BESIII reports the results of the search for $\eta_c \to \pi^+\pi^-$ and $\eta_c \to \pi^0\pi^0$ and upper limits on the branching fractions are presented at the 90% confidence level (C.L.) [4]. In this paper, we present the first experimental search for $\eta_c \to \pi^0\eta'$.

Except for gravitational effects, we still know very little about the constituents and interactions of dark matter. One possible model candidate for dark matter is an additional gauge boson [5,6]. If this additional boson corresponds to an extra $U(1)$ gauge symmetry, it is referred to as a "dark photon." A dark photon with a mass in the sub-GeV range can couple to the SM via kinetic mixing with the ordinary photon and parametrized by the mixing strength [5]. The dark photon occurs naturally in many proposed models and has been invoked to explain various experimental and observational anomalies [7]. This new gauge boson referred to as U' has the same quantum number, $J^{PC} = 1^{--}$, as the ω meson. In the past, BESIII has reported on a search for the dark gauge photon in the initial-state radiation (ISR) reactions $e^+e^- \to U'\gamma_{\rm ISR} \to l^+l^-\gamma_{\rm ISR}$ ($l = \mu,\ e$) [8] and electromagnetic Dalitz decays $J/\psi \to U'\eta/\eta' \to e^+e^-\eta/\eta'$ [9,10]. The same ISR method has been used by the *BABAR* experiment [11]. The BELLE and KLOE Collaborations report a search for a dark vector gauge boson decaying to $\pi^+\pi^-$, where the dark vector gauge boson mass spans a range from 290 to 520 MeV/c^2 [12] and 519 to 973 MeV/c^2 [13], respectively.

In this paper, using a sample of $1.31 \times 10^9 J/\psi$ events collected with the BESIII detector, we present the first study of $J/\psi \to \gamma\pi^0\eta'$, which allows us to search for the CP-violating decay of $\eta_c \to \pi^0\eta'$ and to search for a new gauge boson [5] by investigating the $\gamma\pi^0$-mass spectrum. Additionally, we present the most accurate measurement of the $J/\psi \to \omega\eta'$ branching fraction [current BESIII measurement value is $(2.08 \pm 0.30 \pm 0.14) \times 10^{-4}$ [14]].

II. THE BESIII EXPERIMENT AND MONTE CARLO SIMULATION

The BESIII detector is a cylindrical magnetic spectrometer [15] located at the Beijing Electron Positron Collider (BEPCII) [16], with an acceptance of charged particles and photons of 93% over 4π solid angle. The BESIII detector consists of a helium-based multilayer drift chamber (MDC), a plastic scintillator time-of-flight system (TOF), and a CsI (Tl) electromagnetic calorimeter (EMC), which are all enclosed in a superconducting solenoidal magnet providing a 1.0 T (0.9 T in 2012) magnetic field. The solenoid is supported by an octagonal flux-return yoke with resistive plate counter muon identifier modules interleaved with steel. The charged-particle momentum resolution at 1 GeV/c is 0.5%, and the dE/dx resolution is 6% for the electrons from Bhabha scattering. The EMC measures photon energies with a resolution of 2.5% (5%) at 1 GeV in the barrel (end-cap) region. The time resolution of the TOF barrel part is 68 ps, while that of the end-cap part is 110 ps. Particle identification (PID) for charged pions is performed by exploiting the TOF information and the specific ionization energy loss, dE/dx, measured by the MDC. The TOF and dE/dx information is combined to form PID probability for the pion, kaon, and proton hypotheses; each track is assigned to the particle type that corresponds to the hypothesis with the highest probability.

Simulated samples produced with the GEANT4-based [17] Monte Carlo (MC) package, which includes the geometric description [18,19] of the BESIII detector and the detector response, are used to determine the detection efficiency and to estimate the backgrounds. The inclusive MC sample consists of the production of the J/ψ resonance, and the continuum processes incorporated in KKMC [20].

The known decay modes are generated using the EVTGEN package [21] using branching fractions taken from the Particle Data Group (PDG) [22], and the remaining unknown decays from the charmonium states with the LUNDCHARM package [23]. The final-state radiations from charged final-state particles are incorporated with the PHOTOS package [24].

The three-body decay of $J/\psi \to \gamma\pi^0\eta'$ without any intermediate states is simulated with a model based on a phase-space distribution of the final-state particles. The decays of $J/\psi \to \gamma\eta_c, U'\eta', \gamma\eta'$, and $\omega\eta'$ are generated with an angular distribution of $1 + \cos^2\theta_\gamma$, where θ_γ is the angle of radiative photon relative to the positron beam direction in the J/ψ-rest frame, while the subsequent $\eta_c(\eta')$ decays are generated with a phase-space model and the $U'(\omega) \to \gamma\pi^0$ decay is modeled by a P-wave [21].

III. EVENT SELECTION

Candidates of $J/\psi \to \gamma\pi^0\eta', \eta' \to \pi^+\pi^-\eta, \pi^0 \to \gamma\gamma, \eta \to \gamma\gamma$ are required to have two oppositely charged tracks and at least five photon candidates. All charged tracks must originate from the interaction point with a distance of closest approach less than 10 cm in the beam direction and less than 1 cm in the transverse plane. Their polar angles, θ, with respect to the beam direction are required to satisfy $|\cos\theta| < 0.93$.

Electromagnetic showers are reconstructed from clusters of firing EMC crystals. The energy deposited in nearby TOF counters is included to improve the reconstruction efficiency and energy resolution. The showers of the photon candidate must have a minimum energy of 25 MeV in the barrel region ($|\cos\theta_\gamma| < 0.80$) and 50 MeV in the end-cap region ($0.86 < |\cos\theta_\gamma| < 0.92$), where θ_γ is the polar angle of the photon. To suppress showers originating from charged particles, a photon candidate must be separated by at least 10° from the nearest charged track. To suppress noise and energy deposits unrelated to the event, the time at which the photon is recorded in the EMC after the e^+e^- collision is required to be within $0 \le t \le 700$ ns.

After selecting the charged tracks and showers, a four-constraint (4C) kinematic fit to the $J/\psi \to \pi^+\pi^-5\gamma$ hypothesis is performed using energy-momentum conservation. For events with more than five photon candidates, the combination with the smallest χ^2_{4C} is retained. To suppress background events with six photons in the final states, the χ^2_{4C} of the $\pi^+\pi^-5\gamma$ hypothesis is required to be less than that for the $\pi^+\pi^-6\gamma$ hypothesis.

To distinguish the photon from π^0 and η decays, we define the variable $\chi^2_{\pi^0\eta} \equiv (\frac{M_{\gamma\gamma}-m_{\pi^0}}{\sigma_{\pi^0}})^2 + (\frac{M_{\gamma\gamma}-m_\eta}{\sigma_\eta})^2$. This variable is used to choose from the five photon candidates two pairs of photons with two-photon invariant masses ($M_{\gamma\gamma}$) closest to the nominal π^0 (m_{π^0}) and η (m_η) masses. σ_{π^0} (σ_η) refers to the experimental mass resolution for a π^0 (η) decay. The four-photon combination with the smallest value for $\chi^2_{\pi^0\eta}$ is chosen.

To improve the mass resolution and to further suppress background events, we subsequently perform a five-constraint kinematic (5C) fit imposing energy-momentum conservation and an η-mass constraint under the hypothesis of $\pi^+\pi^-\gamma\gamma\gamma\eta$, where the η candidate is reconstructed with the selected pair of photons as described above. Events with a χ^2_{5C} less than 30 are accepted for further analysis.

To select π^0 candidates, the invariant mass of the two photons from π^0 decay, $M_{\gamma\gamma}$, must satisfy $|M_{\gamma\gamma} - m_{\pi^0}| < 15\ \mathrm{MeV}/c^2$. To suppress background events with multi-π^0 in the final states, we require that the invariant mass of the radiative photon and any photon from the η decay is outside the π^0-mass region of $[0.115, 0.155]\ \mathrm{GeV}/c^2$. To select η' candidates, we calculate for each event the $\pi^+\pi^-\eta$ invariant mass, $M_{\pi^+\pi^-\eta}$, and require that $|M_{\pi^+\pi^-\eta} - m_{\eta'}| < 15\mathrm{MeV}/c^2$, where $m_{\eta'}$ is the nominal η' mass.

IV. SEARCH FOR $\eta_c \to \pi^0\eta'$

After applying the selection criteria, we obtain the $\pi^0\eta'$ invariant-mass distribution as shown in Fig. 1. No evident η_c peak is seen. We found that the dominant background events are from decays with the η' as an intermediate state, such as $J/\psi \to \gamma\pi^0\eta'$, $J/\psi \to \omega\eta'$, and $J/\psi \to \gamma\eta'$, and the corresponding contributions are displayed in Fig. 1(a) as well. Other background contributions (non-η' background) are estimated from events for which the reconstructed η' mass falls within the η'-sideband regions ($0.903 < M_{\pi^+\pi^-\eta} < 0.933\mathrm{GeV}/c^2$ and $0.983 < M_{\pi^+\pi^-\eta} < 1.013\mathrm{GeV}/c^2$). The sum of the above contributions gives a reasonable description of the data.

An unbinned maximum-likelihood fit is performed to determine the signal yield as shown in Fig. 1(b). In the fit, the probability density function (PDF) of the signal is described by a MC simulated shape and the widths and masses are fixed to the world average values taken from the PDG [22]. The background shape from the $J/\psi \to \gamma\eta'$ channel is described with a MC simulated shape, and the yield is fixed according to the published branching fractions [22]. The other nonpeaking background is described by a first-order Chebyshev polynomial function. The signal yield is $N_{\mathrm{sig}} = 7.2 \pm 7.6$ and the statistical significance of the η_c signal is calculated to be 1.0σ using $\sqrt{-2\ln(\mathcal{L}_0^{\mathrm{stat}}/\mathcal{L}_{\mathrm{max}}^{\mathrm{stat}})}$, where $\mathcal{L}_{\mathrm{max}}^{\mathrm{stat}}$ and $\mathcal{L}_0^{\mathrm{stat}}$ are the maximum-likelihood values with the signal yield left free and fixed at zero, respectively. In addition, to account for the additive systematic uncertainties related to the fits, the fit range and the background shape are varied and the maximum signal yield among these cases is obtained as shown in Fig. 1(b).

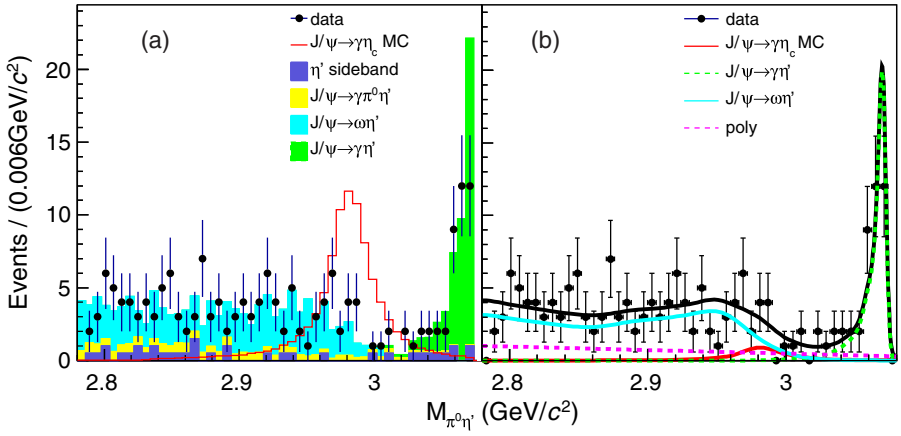

FIG. 1. The $\pi^0\eta'$-mass spectrum. The black dots with error bars are data. (a) The histogram with the red line represents the extracted line shape of the signal process $J/\psi \to \gamma\eta_c$. The yellow area shows the MC distribution of $J/\psi \to \gamma\pi^0\eta'$, the green area corresponds to the MC distribution of $J/\psi \to \gamma\eta'$, the blue area shows the MC distribution of $J/\psi \to \omega\eta'$, and the gray area represents the non-η' contributions obtained from η'-sideband data. (b) Fit to the $M_{\pi^0\eta'}$ with a free signal yield. The red histogram shows the contribution of the η_c signal, the green dashed line represents the $J/\psi \to \gamma\eta'(\eta' \to \eta\pi^+\pi^-, \eta \to \gamma\gamma)$ background contribution, and the pink dashed line depicts other nonpeaking background contributions described by a first-order Chebyshev polynomial.

V. SEARCH FOR DARK PHOTON IN $U' \to \gamma\pi^0$ DECAY

Using the same selection criteria as used to search for $\eta_c \to \pi^0\eta'$, we study the $\gamma\pi^0$-mass ($M_{\gamma\pi^0}$) distribution as shown in Fig. 2. A clear ω peak from $J/\psi \to \omega\eta'$ decays can be observed. There is also a small background contribution from $J/\psi \to \gamma\eta'$ decays which is smoothly distributed in the low-mass region of the $M_{\gamma\pi^0}$ distribution. The contributions from non-η' backgrounds are described by events that are selected in the η'-sideband regions, $0.903 < M_{\pi^+\pi^-\eta} < 0.933$ GeV/c^2 and $0.983 < M_{\pi^+\pi^-\eta} < 1.013$ GeV/c^2.

We search for the U' signal in steps of 10 MeV/c^2 in the $M_{\gamma\pi^0}$ distribution ranging from 0.2 to 2.1 GeV/c^2 and excluding the mass region around the ω peak (0.75 to 0.82 GeV/c^2). The mass resolution of a U' signal has been evaluated using signal MC events generated at 183 different U'-mass ($M_{U'}$) hypotheses points with a negligible width. Depending upon the U' mass, the resolutions vary in the range between 3.6 and 10.4 MeV/c^2. We perform a series of unbinned extended maximum-likelihood fits to the $M_{\gamma\pi^0}$ distribution to determine the number of signal candidates as a function of $M_{U'}$ in the interval of $0.2 \le M_{U'} \le 2.1$ GeV/c^2. The fit range is varied with the different signal mass points. In general, the fit range is $[M_{U'} - 0.1, M_{U'} + 0.1]$ GeV/c^2. To handle the threshold-mass region and peaking background smoothly, the fit range is [0.15, 0.35], [0.55, 0.75], [0.82, 1.02], and [1.95, 2.15] GeV/c^2 for $0.2 \le M_{U'} \le 0.35$, $0.65 \le M_{U'} \le 0.74$, $0.83 \le M_{U'} \le 0.92$, and $2.05 \le M_{U'} \le 2.1$ GeV/c^2, respectively. The U' signal and the tail of the ω signal are described by MC-simulated shapes, and the remaining background contribution is modeled with a linear Chebyshev polynomial. To take into account the additive systematic uncertainties related to the fits, alternative fits with different fit range and background shape are also performed, and the maximum upper limit among these cases has been selected. The number of extracted signal events, the significance, and the detection efficiency as a function of $M_{U'}$ are shown in Fig. 3. The largest local significance defined as before is computed to be 2.4σ at $M_{U'} = 1.78$ GeV/c^2, the corresponding p-value is calculated to be 0.89. No significant signal for $U' \to \gamma\pi^0$ is found.

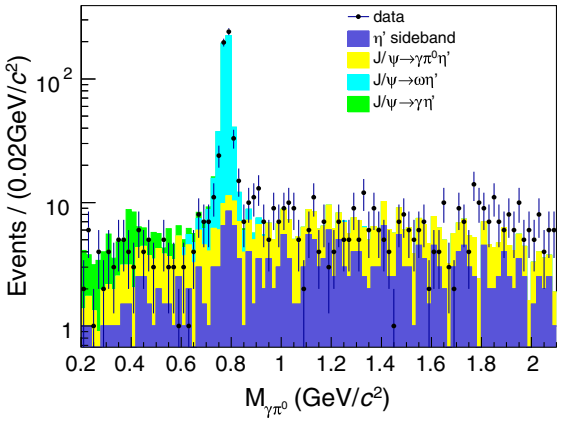

FIG. 2. The $\gamma\pi^0$ invariant-mass spectrum. The black dots with error bars are data. The various shaded histograms are described in the caption of Fig. 1(a).

VI. BRANCHING FRACTION MEASUREMENT OF $J/\psi \to \omega\eta'$

Figure 4 shows the mass distribution of $M_{\pi^+\pi^-\eta}$ versus $M_{\gamma\pi^0}$. Events originating from the $J/\psi \to \omega\eta'$ decay are

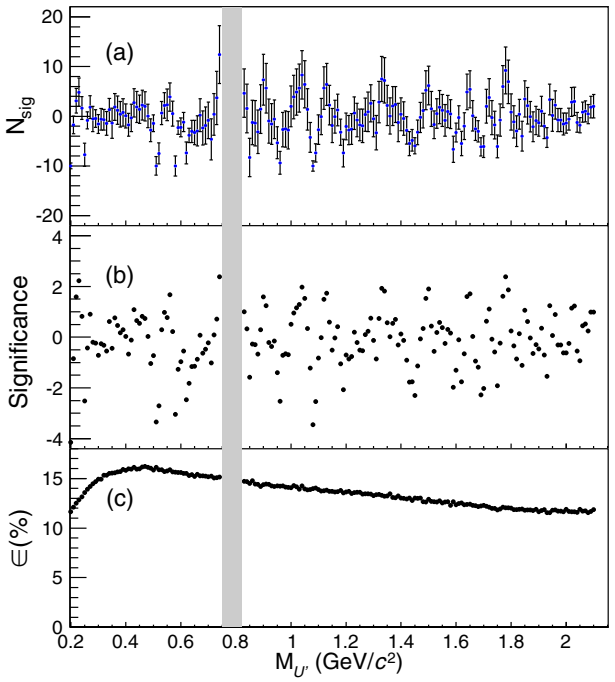

FIG. 3. (a) The number of extracted signal events, (b) Statistical signal significance, and (c) the detection efficiency as a function of $M_{U'}$ in the range of $0.2 \leq M_{U'} \leq 2.1$ GeV/c^2. The region of the ω resonance is indicated by the gray band and excluded from the U' search.

clearly visible. To extract the number of $\omega\eta'$ events, an unbinned extended maximum-likelihood fit using a two-dimensional (2D) PDF including both variables, $M_{\pi^+\pi^-\eta}$ and $M_{\gamma\pi^0}$, with the requirements of $0.6 < M_{\gamma\pi^0} < 1.0$ GeV/c^2 and $0.908 < M_{\pi^+\pi^-\eta} < 1.008$ GeV/c^2 is performed. Assuming zero correlation between the two discriminating variables $M_{\gamma\pi^0}$ and $M_{\pi^+\pi^-\eta}$, the composite PDF in the 2D fit is constructed as follows:

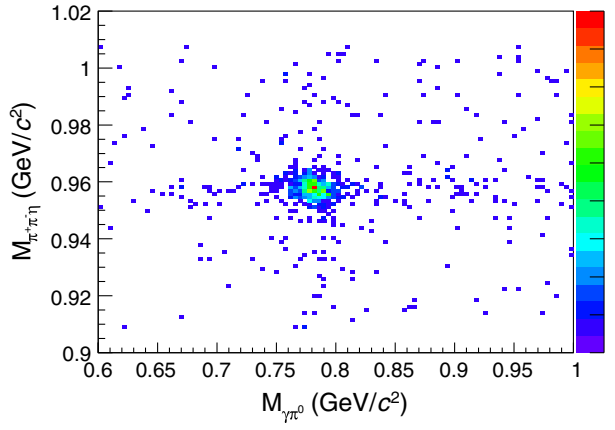

FIG. 4. A two-dimensional distribution of the reconstructed $\pi^+\pi^-\eta$ and $\gamma\pi^0$ masses. The size of each box scales with the number of events found in that particular bin.

$$
\begin{aligned}
F = {} & N_{\rm sig} \times (F^{\omega}_{\rm sig} \cdot F^{\eta'}_{\rm sig}) \\
& + N^{\rm non-\omega}_{\rm bkg} \times (F^{\eta'}_{\rm sig} \cdot F^{\rm non-\omega}_{\rm bkg}) \\
& + N^{\rm non-\eta'}_{\rm bkg} \times (F^{\omega}_{\rm sig} \cdot F^{\rm non-\eta'}_{\rm bkg}) \\
& + N^{\rm non-\omega\eta'}_{\rm bkg} \times (F^{\rm non-\omega}_{\rm bkg} \cdot F^{\rm non-\eta'}_{\rm bkg}),
\end{aligned}
$$

where the signal shapes for the ω ($F^{\omega}_{\rm sig}$) and η' ($F^{\eta'}_{\rm sig}$) responses are modeled with a relativistic Breit-Wigner function convoluted with a Gaussian function. The widths and masses of the ω and η' are fixed in the fit. The parameters of the Gaussian function are free in the fit. $N_{\rm sig}$ is the number of $J/\psi \to \omega\eta', \omega \to \gamma\pi^0, \eta' \to \pi^+\pi^-\eta$ signal events. The backgrounds are divided into three categories, namely non-ω peaking background, non-η' peaking background, and non-$\omega\eta'$ background. The parameters $N^{\rm non-\omega}_{\rm bkg}$, $N^{\rm non-\eta'}_{\rm bkg}$, and $N^{\rm non-\omega\eta'}_{\rm bkg}$ are the corresponding three background yields. The background shapes, $F^{\rm non-\omega}_{\rm bkg}$ and $F^{\rm non-\eta'}_{\rm bkg}$, related to $M_{\gamma\pi^0}$ and $M_{\pi^+\pi^-\eta}$, respectively, are described by first-order Chebyshev polynomials and all their corresponding parameters are free in the fit.

The fit results in $N_{\rm sig} = 506 \pm 25$ signal events. The projection plots of the fit on the $M_{\gamma\pi^0}$ and $M_{\pi^+\pi^-\eta}$ distributions are shown in Figs. 5(a) and 5(b), respectively.

VII. SYSTEMATIC UNCERTAINTY

The sources of systematic uncertainties and their corresponding contributions to the measurements of the upper limits and branching fraction are summarized in Table I.

The uncertainty of the number of J/ψ events is determined to be 0.54% by an analysis of inclusive hadronic events in J/ψ decays [25].

The uncertainty of the MDC tracking efficiency for each charged pion is studied by analyzing a nearly background-free sample of $J/\psi \to \rho\pi$ events. The difference between the data and MC simulation is less than 1.0% for each charged track [26] whose value is taken as a systematic uncertainty. Similarly, the uncertainty related to the PID efficiencies of pions is also studied with the data sample, $J/\psi \to \rho\pi$, and the average difference of the PID efficiencies between data and MC simulation is determined to be 1.0% for each charged pion, which is then taken as the corresponding systematic uncertainty. The photon detection efficiency is studied with the control sample $J/\psi \to \pi^+\pi^-\pi^0$ [27]. The difference in efficiency between the data and that predicted by MC simulations is found to be 0.5% per photon in the EMC barrel and 1.5% per photon in the end-cap part of the EMC. In our case, the uncertainty is on average 0.6% per photon whose value is obtained by weighting the uncertainties according to the angular distribution of the five photons found in our data sample. Thus, the uncertainty associated with the five reconstructed photons is 3.0%.

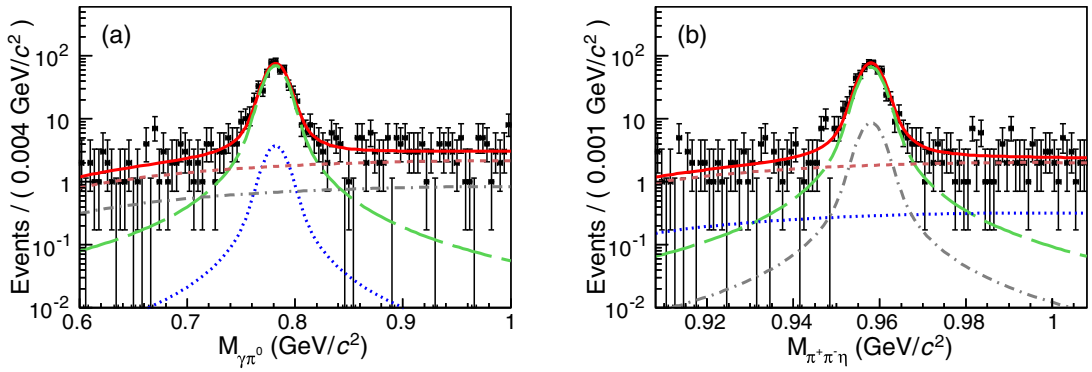

FIG. 5. Projection plots of (a) $M_{\gamma\pi^0}$ and (b) $M_{\pi^+\pi^-\eta}$ distributions in the decay chain of $J/\psi \to \omega\eta', \omega \to \gamma\pi^0, \eta' \to \pi^+\pi^-\eta$. The dots with error bars correspond to data; the solid curve shows the result of the fit including both signal and background distributions. The long-dashed curve corresponds to the contribution of the $\omega\eta'$ signal, the dotted curve shows the contribution of the non-η' peaking background, the dot-dashed curve shows the contribution of the non-ω peaking background, and the short-dashed curve represents the non-$\omega\eta'$ background part.

The uncertainty associated with the 5C kinematic fits comes from the inconsistency of the track helix parameters between the data and MC simulation. The helix parameters for the charged tracks of MC samples are corrected to eliminate part of the inconsistency, as described in Ref. [28]. We take half of the differences on the selection efficiencies with and without the correction as an estimate of the corresponding systematic uncertainties, which results in 0.4%.

Due to the difference in the mass resolution between the data and MC, the uncertainty related to the η' and π^0 mass-window requirements is investigated by smearing the MC simulation in accordance with the signal shape of the data.

TABLE I. The systematic uncertainties for the (product) branching fractions of the two upper-limit studies (η_c and U') and of the $J/\psi \to \omega\eta'$ channel. All values are given in percentage.

Source	η_c	U'	$J/\psi \to \omega\eta'$
Number of J/ψ events	0.54	0.54	0.54
MDC tracking	2.0	2.0	2.0
Particle identification	2.0	2.0	2.0
Photon reconstruction	3.0	3.0	3.0
5C kinematic fit	0.4	0.4	0.4
η' mass window	0.2	0.2	0.2
π^0 mass window	1.1	1.1	1.1
MC efficiency	1.0	1.0	1.0
Fit range	...	...	1.8
Background shape	...	...	0.6
2D fit	...	...	1.4
π^0 veto	1.1	1.1	1.1
$\mathcal{B}(J/\psi \to \gamma\eta_c)$	23.5	...	...
$\mathcal{B}(\omega \to \gamma\pi^0)$	...	...	3.4
$\mathcal{B}(\eta' \to \pi^+\pi^-\eta)$	1.6	1.6	1.6
$\mathcal{B}(\eta \to \gamma\gamma)$	0.5	0.5	0.5
$\mathcal{B}(\pi^0 \to \gamma\gamma)$	0.03	0.03	0.03
Total	24.0	4.9	6.4

The difference of the detection efficiency before and after smearing is assigned as the systematic uncertainty for the η' and π^0 mass-window requirements and found to be 0.2% and 1.1%, respectively.

The systematic uncertainty related to the finite statistics used by the MC simulation to obtain the overall reconstruction efficiency is calculated as $\sqrt{\frac{\epsilon(1-\epsilon)}{n}}$, where ϵ is the detection efficiency and n is the number of generated MC events of the signal process. The corresponding systematic uncertainty is determined to be 1.0%.

The systematic uncertainties that affect the upper limits on the branching fraction of $\eta_c \to \pi^0\eta'$ and $U' \to \gamma\pi^0$ are considered in two categories: additive and multiplicative. The additive systematic uncertainties on the fit range and background shapes are already accounted for in the analysis procedure that is applied to obtain the maximum upper limit of the signal yield. Therefore, here we only consider these uncertainties for the $J/\psi \to \omega\eta'$ study. To study the uncertainty from the fit range, the fit is repeated with different fit ranges, and the largest difference in the signal yield, 1.8%, is taken as the systematic uncertainty. The uncertainty associated with the background shape in the fits to the $M_{\gamma\pi^0}$ distribution is estimated using alternative fits by changing the linear Chebyshev polynomial to a second-order Chebyshev polynomial. The difference in signal yield (0.6%) is taken as the systematic uncertainty.

The uncertainty associated with the 2D fits of the $J/\psi \to \omega\eta'$ channel is estimated by taking all parameters as free parameters in the fit. The change in signal yield (1.4%) is taken as the systematic uncertainty. The systematic uncertainty due to the π^0 veto is evaluated by varying the requirement on the mass window, and the difference in yield compared to the nominal choice (1.1%) is assigned as the systematic uncertainty.

The branching fractions of the intermediate processes of $J/\psi \to \gamma\eta_c$, $\omega \to \gamma\pi^0$, $\eta' \to \pi^+\pi^-\eta$, $\eta \to \gamma\gamma$, and $\pi^0 \to \gamma\gamma$

are taken from the PDG [22] and their errors are considered as a source of systematic uncertainty.

For each case, the total systematic uncertainty is given by the quadratic sum of the individual contributions, assuming all sources to be independent.

VIII. RESULTS

Since no evident η_c signal is seen in $M_{\pi^0\eta'}$, a Bayesian method is used to obtain the upper limit of the signal yield at the 90% C.L. To determine the upper limit on the η_c signal, a series of unbinned maximum-likelihood fits are performed to the $\pi^0\eta'$-mass spectrum with a varying number of expected η_c signals. From this, we obtain the dependence of the likelihood on the number of signal events from which we extract the upper limit, taking into account the multiplicative systematic uncertainties as follows [29]:

$$\mathcal{L}'(\mathcal{B}) = \int_{-\infty}^{+\infty} \mathcal{L}^{\rm stat}(\mathcal{B}') e^{-\frac{\Delta^2}{2\sigma^2_{\rm syst}}} d\Delta. \quad (1)$$

Here, $\mathcal{L}^{\rm stat}$ and $\mathcal{L}'$ are the likelihood curves before and after the inclusion of the multiplicative systematic uncertainty. $\mathcal{B}' = (1+\Delta)\mathcal{B}$, where Δ is the relative deviation of the estimated branching fraction from the nominal value, and $\sigma_{\rm syst}$ is the multiplicative systematic uncertainties given in Table I.

The branching fraction for a particular decay process is computed as

$$\mathcal{B}(X \to Y) = \frac{N_{\rm sig}}{\epsilon \times \mathcal{B}},$$

where $N_{\rm sig}$ is the number of extracted signal yield, ϵ is the signal selection efficiency, and $\mathcal{B}$ is the secondary branching fraction of the corresponding decay process.

The normalized likelihood distribution for $J/\psi \to \gamma\eta_c(\eta_c \to \pi^0\eta')$ candidates is shown in Fig. 6. The upper limit at the 90% C.L. of the signal yield ($N_{\rm UL}$) and detection efficiency are determined to be 19.0% and 9.3% respectively, resulting in a branching fraction $\mathcal{B}(\eta_c \to \pi^0\eta')$ of less than 5.6×10^{-5}.

Due to no evident U' signal seen in $M_{\gamma\pi^0}$, we compute the upper limit on the product branching fraction $\mathcal{B}(J/\psi \to U'\eta') \times \mathcal{B}(U' \to \pi^0\gamma)$ at the 90% C.L. as a function of $M_{U'}$ using a Bayesian method after incorporating the systematic uncertainty by smearing the likelihood curve with a Gaussian function with a width of the systematic uncertainty as follows:

$$\mathcal{L}^{\rm smear}(\mathcal{B}) = \int \mathcal{L}\left(\frac{\epsilon}{\bar{\epsilon}}\mathcal{B}\right) e^{-\frac{(\epsilon-\bar{\epsilon})^2}{2\sigma^2_{\epsilon}}} d\epsilon, \quad (2)$$

where, $\mathcal{L}$ and $\mathcal{L}^{\rm smear}$ are the likelihood curves before and after the consideration of the systematic uncertainty. ϵ, $\bar{\epsilon}$, and σ_ϵ are the detection efficiency, nominal efficiency, and the absolute total systematic uncertainty on the efficiency, respectively. As shown in Fig. 7, the combined limits on product branching fraction $\mathcal{B}(J/\psi \to U'\eta') \times \mathcal{B}(U' \to \pi^0\gamma)$ are established at the level of $(0.8\text{–}6.5) \times 10^{-7}$ for $0.2 \le M_{U'} \le 2.1$ GeV/c^2.

With a detection efficiency of 14.9% obtained from a MC simulation, we obtain a branching fraction for the $J/\psi \to \omega\eta'$ process of $(1.87 \pm 0.09 \pm 0.12) \times 10^{-4}$, where the first uncertainty is statistical and the second systematic.

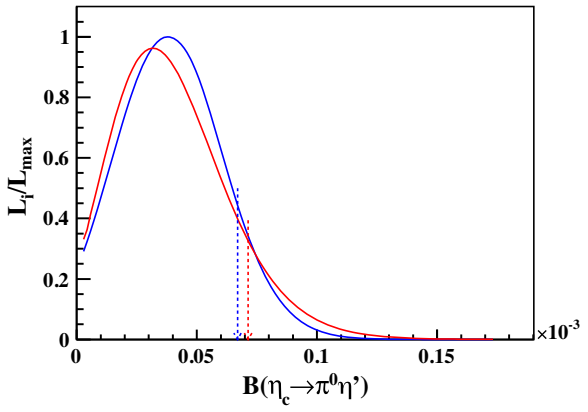

FIG. 6. The distribution of the normalized likelihood scan for $J/\psi \to \gamma\eta_c(\eta_c \to \pi^0\eta')$ candidates. The blue and red curves describe the smoothed likelihood curves before and after the inclusion of the multiplicative systematic uncertainty. The blue and red arrows show the upper limit on the signal yield at 90% C.L.

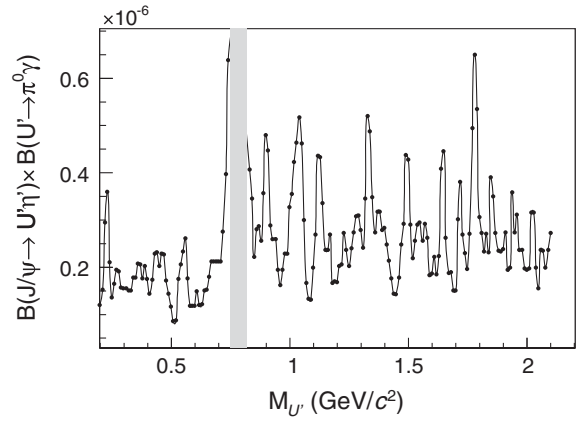

FIG. 7. The upper limit at the 90% C.L. on the product branching fraction $\mathcal{B}(J/\psi \to U'\eta') \times \mathcal{B}(U' \to \pi^0\gamma)$. The region of the ω resonance indicated by the gray band is excluded from the U' search.

IX. SUMMARY

Using a sample of $(1310.6 \pm 7.0) \times 10^6 J/\psi$ events collected with the BESIII detector, the decay of

$J/\psi \to \gamma\eta'\pi^0$ is studied. We search for the CP-violating decay $\eta_c \to \pi^0\eta'$ and a dark gauge boson U' in $J/\psi \to U'\eta', U' \to \gamma\pi^0, \pi^0 \to \gamma\gamma$. No significant η_c signal is observed in the $\pi^0\eta'$ invariant-mass spectrum, and the upper limit on the branching fraction is determined to be 5.6×10^{-5} at the 90% C.L. Except for a clear ω peak in the $\gamma\pi^0$ mass spectrum, no significant excess is seen for any mass hypothesis in the range of $0.2 \le M_{U'} \le 2.1$ GeV/c^2. The upper limits on the product branching fractions are calculated to be $(0.8\text{–}6.5) \times 10^{-7}$ at the 90% C.L. Due to lack of the theoretical predictions on the $\mathcal{B}(J/\psi \to U'\eta')$, we do not present the upper limit on the coupling of the dark vector gauge boson. In case of corresponding theoretical calculations in the future, we would like to present the detailed information, e.g., the detection efficiency, signal yield, and branching fraction, as shown in Tables II and III in the Appendix. The detection efficiencies increase first and then decrease, and the jumping of individual points is within the range of statistical error. In this case, it would be easy for readers or theorists to extract the coupling in case the corresponding prediction is available.

In addition, the branching fraction of $J/\psi \to \omega\eta'$ is measured to be $(1.87 \pm 0.09 \pm 0.12) \times 10^{-4}$, where the first uncertainty is statistical and the second systematic. This result is consistent with the previously published BESIII measurement but with an improvement in accuracy by a factor of 1.4.

ACKNOWLEDGMENTS

The BESIII Collaboration thanks the staff of BEPCII and the IHEP computing center for their strong support. This work is supported in part by National Key Basic Research Program of China under Contract No. 2015CB856700; National Natural Science Foundation of China (NSFC) under Contracts No. 11625523, No. 11635010, No. 11675184, No. 11735014, No. 11822506, No. 11835012; the Chinese Academy of Sciences (CAS) Large-Scale Scientific Facility Program; Joint Large-Scale Scientific Facility Funds of the NSFC and CAS under Contracts No. U1532257, No. U1532258, No. U1732263, No. U1832207; CAS Key Research Program of Frontier Sciences under Contracts No. QYZDJ-SSW-SLH003, No. QYZDJ-SSW-SLH040; 100 Talents Program of CAS; INPAC and Shanghai Key Laboratory for Particle Physics and Cosmology; ERC under Contract No. 758462; German Research Foundation DFG under Contracts No. Collaborative Research Center CRC 1044, No. FOR 2359; Istituto Nazionale di Fisica Nucleare, Italy; Koninklijke Nederlandse Akademie van Wetenschappen under Contract No. 530-4CDP03; Ministry of Development of Turkey under Contract No. DPT2006K-120470; National Science and Technology fund; STFC (United Kingdom); The Knut and Alice Wallenberg Foundation (Sweden) under Contract No. 2016.0157; The Royal Society, UK under Contracts No. DH140054, No. DH160214; The Swedish Research Council; U.S. Department of Energy under Contracts No. DE-FG02-05ER41374, No. DE-SC-0010118, No. DE-SC-0012069; University of Groningen and the Helmholtzzentrum fuer Schwerionenforschung GmbH, Darmstadt.

APPENDIX

TABLE II. The results of signal yield (N_{sig}), the upper limit at the 90% C.L. of the signal yield (N_{UL}), efficiency (ϵ), and branching fraction ($\mathcal{B}$) as a function of $M_{U'}$.

$M_{U'}$	N_{sig}	N_{UL}	ϵ (%)	$\mathcal{B}(10^{-7})$
0.20	−10.00	2.50	11.63	1.19
0.21	−1.74	3.80	12.10	1.52
0.22	3.12	7.20	12.52	2.94
0.23	4.84	9.20	12.84	3.58
0.24	1.64	5.90	13.14	2.10
0.25	−7.74	3.30	13.58	1.36
0.26	−0.82	4.30	13.92	1.65
0.27	1.83	6.00	14.20	1.94
0.28	−0.53	5.30	14.47	1.91
0.29	−0.44	4.30	14.69	1.57
0.30	−1.55	4.20	14.92	1.54
0.31	−0.61	4.70	14.92	1.54
0.32	−0.70	4.60	15.33	1.50
0.33	−1.42	5.00	15.33	1.50
0.34	1.29	5.70	15.52	1.78
0.35	−1.39	5.70	15.54	1.78
0.36	1.86	6.70	15.57	2.07
0.37	1.22	6.70	15.66	2.06
0.38	0.43	5.90	15.69	1.76
0.39	0.77	6.30	15.91	2.02
0.40	0.07	5.40	15.82	1.74
0.41	−1.73	4.70	15.98	1.44
0.42	−0.32	5.80	15.94	1.73
0.43	2.71	7.60	16.12	2.28
0.44	1.88	7.40	15.94	2.31
0.45	1.41	6.80	15.98	2.02
0.46	2.25	7.50	16.15	2.28
0.47	1.99	7.20	16.22	2.27
0.48	0.06	5.40	16.13	1.71
0.49	−2.79	4.30	16.03	1.44
0.50	−1.42	3.80	15.86	1.16
0.51	−10.00	2.80	16.12	0.86
0.52	−7.47	3.00	15.88	0.87
0.53	0.65	5.40	15.89	1.74
0.54	2.17	6.70	15.70	2.05
0.55	2.28	7.80	15.76	2.33
0.56	3.89	8.40	15.87	2.61
0.57	0.54	5.80	15.65	1.76
0.58	−10.00	3.40	15.64	1.18
0.59	−2.31	3.40	15.60	1.18
0.60	−2.24	4.00	15.61	1.18
0.61	−1.17	4.20	15.50	1.48

(Table continued)

TABLE II. *(Continued)*

$M_{U'}$	N_{sig}	N_{UL}	ϵ (%)	$\mathcal{B}(10^{-7})$
0.62	−7.38	3.20	15.53	1.19
0.63	−3.06	3.20	15.31	1.20
0.64	−3.29	4.10	15.40	1.49
0.65	−3.29	4.40	15.21	1.51
0.66	−2.95	5.40	15.42	1.79
0.67	0.25	6.90	15.25	2.11
0.68	−2.36	6.20	15.26	2.11
0.69	−1.88	6.70	15.22	2.12
0.70	−0.82	6.90	15.16	2.12
0.71	−4.64	6.60	15.22	2.12
0.72	0.37	8.50	15.06	2.75
0.73	3.69	12.40	15.08	3.97
0.74	12.38	19.90	15.15	6.38
0.83	4.64	12.10	14.72	4.06
0.84	1.57	10.10	14.68	3.45
0.85	−8.30	6.60	14.50	2.22
0.86	−1.23	8.10	14.79	2.80
0.87	−1.40	8.10	14.45	2.87
0.88	−3.14	7.40	14.41	2.55
0.89	1.43	10.30	14.20	3.56
0.90	7.34	14.90	14.39	4.80
0.91	5.66	13.30	14.44	4.46
0.92	−0.98	8.30	14.39	2.88
0.93	−1.56	7.50	14.25	2.58
0.94	−0.60	7.50	14.20	2.59
0.95	−5.33	5.10	14.24	1.94
0.96	−9.37	4.10	14.21	1.62
0.97	−2.67	5.90	14.26	1.94
0.98	−2.55	6.30	14.14	2.28
0.99	−2.81	6.60	14.10	2.28
1.00	2.01	9.20	14.08	3.27
1.01	3.87	10.90	14.30	3.54
1.02	4.89	12.20	14.15	4.23
1.03	5.66	13.10	13.92	4.63
1.04	8.32	15.40	14.24	5.17
1.05	6.43	13.50	13.95	4.62
1.06	1.38	8.90	13.84	2.99
1.07	−4.23	5.00	13.88	1.66
1.08	−10.00	3.10	13.97	1.32
1.09	−7.37	3.30	14.04	1.31
1.10	−2.69	5.20	13.87	1.99
1.11	−0.08	7.40	13.72	2.68
1.12	5.65	12.10	13.76	4.35
1.13	6.38	12.70	13.82	4.33
1.14	2.24	9.20	13.71	3.36
1.15	−1.88	6.50	13.69	2.35
1.16	−0.08	6.90	13.63	2.36
1.17	1.26	7.20	13.67	2.69
1.18	−3.22	4.90	13.79	1.67
1.19	−7.40	4.20	13.54	1.70
1.20	−2.07	5.00	13.64	1.69
1.21	−2.78	5.20	13.71	2.01
1.22	−2.57	5.60	13.48	2.05
1.23	0.62	7.00	13.58	2.71
1.24	−0.75	6.60	13.62	2.37
1.25	−1.74	6.00	13.62	2.03
1.26	−1.94	6.20	13.44	2.40
1.27	0.31	7.10	13.45	2.74
1.28	0.89	8.30	13.47	3.07
1.29	2.61	9.00	13.43	3.08
1.30	−0.49	7.10	13.26	2.77
1.31	−3.31	6.10	13.35	2.41
1.32	2.85	9.80	13.38	3.44
1.33	7.50	14.10	13.29	5.19
1.34	7.22	13.90	13.21	4.87
1.35	2.18	9.30	13.24	3.48
1.36	0.06	7.60	13.46	2.74
1.37	2.04	8.90	13.09	3.16
1.38	2.38	8.60	13.05	3.17
1.39	−1.23	7.20	13.23	2.78
1.40	0.41	7.10	13.03	2.82
1.41	−0.45	6.70	12.99	2.48
1.42	−2.84	5.00	12.92	2.14
1.43	−5.48	4.00	13.02	1.77
1.44	−4.84	3.70	12.77	1.44
1.45	−5.94	3.30	13.01	1.41
1.46	−3.24	4.40	13.01	1.77
1.47	−0.22	6.20	13.03	2.47
1.48	1.15	7.80	12.65	2.91
1.49	5.22	11.20	12.63	4.37
1.50	6.18	11.90	12.90	4.28
1.51	1.47	7.90	12.70	2.90
1.52	−1.71	5.70	12.66	2.18
1.53	0.54	6.60	12.64	2.55

(Table continued)

TABLE III. The results of signal yield (N_{sig}), the upper limit at the 90% C.L. of the signal yield (N_{UL}), efficiency (ϵ), and branching fraction ($\mathcal{B}$) as a function of $M_{U'}$.

$M_{U'}$	N_{sig}	N_{UL}	ϵ (%)	$\mathcal{B}(10^{-7})$
1.54	1.83	7.80	12.74	2.89
1.55	1.17	7.30	12.53	2.94
1.56	−0.82	6.40	12.61	2.55
1.57	0.97	7.20	12.67	2.90
1.58	0.45	6.30	12.29	2.62
1.59	−6.66	4.00	12.64	1.82
1.60	−3.25	4.00	12.36	1.86
1.61	−0.25	5.10	12.46	2.22
1.62	−5.50	4.10	12.53	1.84
1.63	−1.97	5.40	12.36	2.23
1.64	4.89	10.40	12.39	4.08
1.65	5.42	11.00	12.42	4.45
1.66	0.09	6.60	12.29	2.62
1.67	−2.54	4.60	12.25	1.88
1.68	−3.04	4.10	12.16	1.89
1.69	−6.16	3.30	12.23	1.50
1.70	−6.10	3.80	12.28	1.50
1.71	2.02	8.00	12.21	3.02
1.72	3.78	9.80	12.09	3.80
1.73	−0.27	6.90	11.98	2.69
1.74	−1.77	5.30	11.99	2.30
1.75	−6.06	4.10	11.82	1.95
1.76	−0.77	6.40	11.91	2.70
1.77	5.97	12.30	12.10	4.94
1.78	9.23	16.00	12.05	6.49
1.79	6.93	13.40	12.05	5.34
1.80	0.85	8.00	12.03	3.06
1.81	−1.16	6.30	11.87	2.71
1.82	−2.98	5.50.	11.86	2.33
1.83	0.40	6.50	11.90	2.71
1.84	−4.02	5.50	11.93	2.31
1.85	3.49	9.40	11.81	3.90
1.86	2.13	8.60	11.83	3.50
1.87	−0.09	6.50	11.83	2.72
1.88	−2.10	5.60	11.77	2.35
1.89	−0.87	5.70	11.88	2.32
1.90	−1.33	5.40	11.64	2.37
1.91	1.01	6.80	11.76	2.74
1.92	−1.97	5.00	11.86	1.94
1.93	−4.30	4.20	11.56	1.99
1.94	3.36	8.40	11.56	3.58
1.95	0.17	7.00	11.81	2.73
1.96	2.27	7.20	11.83	3.11
1.97	−0.77	5.10	11.70	2.36
1.98	−0.75	5.10	11.69	2.36
1.99	−1.55	4.70	11.66	1.97
2.00	−1.37	4.30	11.88	1.94
2.01	−0.58	4.90	11.69	1.97
2.02	2.87	7.80	11.66	3.16
2.03	2.98	7.70	11.66	3.16
2.04	−1.23	4.40	11.58	1.99
2.05	−1.79	3.80	11.90	1.55
2.06	0.83	5.00	11.72	2.36
2.07	1.01	5.30	11.74	2.35
2.08	0.44	4.80	11.55	1.99
2.09	1.83	5.70	11.67	2.36
2.10	2.02	6.20	11.85	2.72

[1] D. M. Asner *et al.*, Int. J. Mod. Phys. A **24**, 499 (2009).
[2] M. Kobayashi and T. Maskawa, Prog. Theor. Phys. **49**, 652 (1973).
[3] C. Jarlskog and E. Shabalin, Phys. Scr. T **T99**, 23 (2002); E. Shabalin, Phys. Scr. T **T99**, 104 (2002).
[4] M. Ablikim *et al.* (BESIII Collaboration), Phys. Rev. D **84**, 032006 (2011).
[5] P. Fayet, Phys. Lett. **96B**, 83 (1980); P. Fayet and M. Mezard, Phys. Lett. **104B**, 226 (1981); P. Fayet, Nucl. Phys. **B187**, 184 (1981); B. Holdom, Phys. Lett. **166B**, 196 (1986); A. E. Nelson and N. Tetradis, Phys. Lett. B **221**, 80 (1989); P. Fayet, Phys. Rev. D **74**, 054034 (2006); **75**, 115017 (2007); P. Fayet, Phys. Lett. B **675**, 267 (2009); H. B. Li and T. Luo, Phys. Lett. B **686**, 249 (2010); D. Banerjee *et al.* (BESIII Collaboration), Phys. Rev. Lett. **123**, 121801 (2019); R. Aaij *et al.* (LHCb Collaboration), Phys. Rev. Lett. **124**, 041801 (2020).
[6] S. Tulin, Phys. Rev. D **89**, 114008 (2014).
[7] M. Raggi and V. Kozhuharov, Adv. High Energy Phys. **2014**, 959802 (2014).
[8] M. Ablikim *et al.* (BESIII Collaboration), Phys. Lett. B **774**, 252 (2017).
[9] M. Ablikim *et al.* (BESIII Collaboration), Phys. Rev. D **99**, 012006 (2019).
[10] M. Ablikim *et al.* (BESIII Collaboration), Phys. Rev. D **99**, 012013 (2019).
[11] J. P. Lees *et al.* (*BABAR* Collaboration), Phys. Rev. Lett. **113**, 201801 (2014).
[12] E. Won *et al.* (Belle Collaboration), Phys. Rev. D **94**, 092006 (2016).
[13] A. Anastasi *et al.* (KLOE-2 Collaboration), Phys. Lett. B **784**, 336 (2018).
[14] M. Ablikim *et al.* (BESIII Collabotation), Phys. Rev. D **96**, 112012 (2017).
[15] M. Ablikim *et al.* (BESIII Collaboration), Nucl. Instrum. Methods Phys. Res., Sect. A **614**, 345 (2010).

[16] C. H. Yu *et al.*, in *Proceedings of IPAC2016, Busan, Korea, 2016* (JACoW, Geneva, 2016), https://doi.org/10.18429/JACoW-IPAC2016-TUYA01.
[17] S. Agostinelli *et al.* (GEANT4 Collaboration), Nucl. Instrum. Methods Phys. Res., Sect. A **506**, 250 (2003).
[18] Y. T. Liang *et al.*, Nucl. Instrum. Methods Phys. Res., Sect. A **603**, 325 (2009).
[19] B. Huang *et al.*, Chin. Phys. C **32**, 945 (2008).
[20] S. Jadach, B. F. L. Ward, and Z. Was, Phys. Rev. D **63**, 113009 (2001); Comput. Phys. Commun. **130**, 260 (2000).
[21] D. J. Lange, Nucl. Instrum. Methods Phys. Res., Sect. A **462**, 152 (2001); R. G. Ping, Chin. Phys. C **32**, 599 (2008).
[22] M. Tanabashi *et al.* (Particle Data Group), Phys. Rev. D **98**, 030001 (2018), and 2019 update.
[23] J. C. Chen, G. S. Huang, X. R. Qi, D. H. Zhang, and Y. S. Zhu, Phys. Rev. D **62**, 034003 (2000); R. L. Yang, R. G. Ping, and H. Chen, Chin. Phys. Lett. **31**, 061301 (2014).
[24] E. Richter-Was, Phys. Lett. B **303**, 163 (1993).
[25] M. Ablikim *et al.* (BESIII Collaboration), Chin. Phys. C **41**, 013001 (2017).
[26] M. Ablikim *et al.* (BESIII Collaboration), Phys. Rev. Lett. **112**, 251801 (2014).
[27] M. Ablikim *et al.* (BESIII Collaboration), Phys. Rev. D **92**, 052003 (2015).
[28] M. Ablikim *et al.* (BESIII Collaboration), Phys. Rev. D **87**, 012002 (2013).
[29] M. Ablikim *et al.* (BESIII Collaboration), Phys. Lett. B **798**, 135017 (2019).